Nonlinear dynamic elements with noisy sinusoidal forcing: Enhancing response via nonlinear coupling

M. E. Inchiosa* and A. R. Bulsara†
Naval Command, Control and Ocean Surveillance Center, Research, Development, Test and Evaluation Division, Code 573, San Diego, California 92152-5000
(Received 23 December 1994)

We consider a network of nonlinear dynamic elements with nonlinear, global coupling, subject to noise and a time-periodic signal. The system response, characterized by its signal-to-noise ratio, is computed via approximate analytic techniques and precise numerical simulations. We find that cooperative effects arising from the noise and coupling lead to an enhancement of the response of the network over that of a single element.

PACS number(s): 05.40.+j, 02.50.−r, 87.10.+e

I. INTRODUCTION

The presence of a weak periodic signal in a noisy nonlinear dynamic system is known to lead to cooperative stochastic-dynamic effects, including *stochastic resonance*. Stochastic resonance (SR) is a cooperative nonlinear phenomenon wherein the signal-to-noise ratio (SNR) at the output of such a dynamic system, driven by a weak deterministic modulation (which we shall take to be time periodic), can actually be enhanced by increasing the noise. For example, consider a bistable dynamic system where the only information output is a record of switching events between the stable states (attractors) of the potential function underlying the dynamics. When a periodic signal is applied, its effect is to "rock" the potential, alternately raising and lowering the potential wells. If its amplitude is very small compared to the height of the potential barrier, the periodic signal will not be able to induce switching. However, in the presence of even small amounts of Gaussian noise, there will always be a nonzero switching probability. Since the switching probability is greater when the system is in the "elevated" well, which occurs when the signal is at its extrema, one finds that the noise-induced switching events may acquire some degree of coherence with the deterministic signal. The power spectrum obtained from the time-series solution of this system shows sharp peaks at the driving frequency and its odd harmonics (for the case of a symmetric potential), superimposed on a Lorentzian-like noise background. A plot of SNR vs noise strength results in a curve where the SNR first increases up to a maximum value and then falls with increasing noise. In the literature, the SNR vs input noise strength profile is usually taken to be the hallmark of SR. A good overview of the SR phenomenon may be found in recent review articles [1] as well as the proceedings of recent workshops on the subject [2].

A linear filter is known to be the optimal filter for detecting a known sinusoidal signal in Gaussian noise [3]. Despite this, the signal-processing utility of SR has received considerable attention of late due primarily to the notion that in a suitably optimized nonlinear system the gain, which we define as the output SNR (in dB) minus the input SNR, might be positive [4,5]. It is now generally recognized that for a *dynamical* system comprising a single nonlinear element subject to broadband noise, this is not true [6,7]. However, when the noise background is nonwhite, e.g., narrow-band harmonic noise [8,9], positive gains have been observed. Positive gains have also been observed by Grohs *et al.* [10] in an experiment involving optical bistability, with similar noise. In addition, there exists an important class of systems in which it might be possible to obtain enhanced signal detectability in the presence of Gaussian band-limited noise. This is the class of nondynamical or *threshold* systems. In these systems, the response is characterized by crossings of a threshold, in contrast to the (usually bistable) potential dynamics that underpins traditional treatments of SR. Threshold detectors and the zero-crossing problem have been an integral part of the engineering and communications literature [11]. Recently, there has been an upsurge of interest [12,13] in the response of threshold systems due mainly to the realization that they might, in fact, provide a reasonable characterization of the dynamics of neurons and be applicable, for instance, in the physics of nanoscale detection or switching elements.

In this work we consider the performance, quantified by SNR, of a network of nonlinear dynamic elements with *nonlinear*, global coupling. These coupled systems were originally proposed as models, under the appropriate conditions, for neuronal interactions [14]. In this connection it is important to state that although neurons are not, in general, bistable dynamic elements, the coupled bistable dynamics of the form considered throughout this work (i.e., bistability between two fixed points) provides a good model for describing the interaction, in a coarse-grained sense, between the noise and stimulus under conditions that approximate those encountered in real neurons. In fact, bistable dynamics have been shown to account for

*Electronic address: inchiosa@nosc.mil
†Electronic address: bulsara@nosc.mil

many of the experimentally observed features in the dynamics of real neurons [15]. Hence, the ideas developed in this paper should find application in a wide variety of coupled nonlinear dynamic systems, in physics and biology, subject to deterministic stimuli and noise.

Our work is a modification of our earlier work [14] to examine a situation wherein the external sinusoidal signal plus its attendant broadband noise background is incident on *every* element in the array. The coupling between the elements is taken to be of the sigmoidal type to better enable us to draw the connection with analog neural networks. Analytic treatments of the response of such systems are possible only under very restrictive approximations. In this work, we consider a system configuration that lends itself to an approximate treatment via the slaving principle of Haken [16]. The array is taken to consist of a single bistable "reference" element coupled to an ensemble of "bath" elements that evolve on significantly faster time scales than the reference element. Hence, the long-time system behavior is well approximated by the dynamics of the reference element, it being assumed that the bath is never far from equilibrium. Under these conditions, the dynamics of the reference element can be derived in closed form and existing theories [17,18] applied to the computation of the output SNR. In addition to a theoretical characterization of the dynamics (carried out separately for the cases of a bath composed of monostable and bistable elements), we show the results of detailed numerical simulations on the coupled system. The results show that replacing a single nonlinear element by a globally coupled array leads to a significant enhancement in the output SNR. Although the theoretical treatment is restricted in its regime of applicability, it provides a useful qualitative guide for selecting coupling coefficients that maximize the output SNR, even when the conditions necessary for its quantitative validity are violated.

In Sec. II, we describe our model and derive the effective dynamics that characterize the network. Section III contains discussions of the output SNR under various operating scenarios. In particular, we consider the optimum coupling for maximizing the output SNR, and we test the limits of validity of the theory. We introduced these results in preliminary form in [19].

II. COUPLED NONLINEAR DYNAMIC ELEMENTS AND STOCHASTIC RESONANCE

We consider an ensemble of nonlinear dynamic elements, each of which is subject to the same periodic signal embedded in Gaussian white noise $\sqrt{D}\xi(t)$ having mean zero and autocorrelation $D\langle\xi(t)\xi(t+\tau)\rangle = D\delta(\tau)$:

$$C_i\dot{u}_i = -\frac{u_i}{R_i} + \sum_{j=1}^{N} J_{ij}\tanh u_j + \sqrt{D}\xi(t) + q\sin\omega t, \quad (1)$$

the dot denotes the time derivative. Systems of the form (1) have been used to describe connectionist type neural networks [20] with u_i denoting the activation function of the ith element (analogous to the membrane potential of real neurons), and C_i, R_i denoting the input capacitance and transmembrane resistance, respectively. In neural network applications, the coupling coefficients J_{ij}, known as synaptic efficacies, are usually determined via a learning rule.

In the absence of coupling and forcing, the individual elements of the system (1) are bistable for $J_{ii} > (R_iC_i)^{-1}$ and monostable otherwise. The motion of u_i can be visualized as motion in a potential U_i. For $J_{ii} > (R_iC_i)^{-1}$, the potential has wells at $u_i = u_{is\pm}$ separated by a maximum at u_{iu}; otherwise, it has a single well at u_{iu}.

In general, the solution of the above system must be found numerically; however, an approximate analytical formulation for the response of the reference element u_1 may be obtained if we apply some conditions on the allowable parameter values. The bath elements must react at a rate much greater than the rate of change of the reference element or the forcing signal. Therefore, the rate for probability to equilibrate at the bottom of the bath elements' potential wells must be much greater than the rate at the bottom of the reference element's potential well and the rate of the forcing,

$$U_i''(u_{is\pm}) \text{ or } U_i''(u_{iu}) \ll U_1''(u_{1s\pm}), \omega, \quad (i > 1). \quad (2)$$

Furthermore, the cross coupling and forcing terms should not be so large that they overwhelm the basic monostable or bistable dynamics of the elements,

$$q, \sum_{j\neq i} |J_{ij}| \ll \max(1/R_i, |J_{ii}|). \quad (3)$$

These conditions constitute the cornerstone of the adiabatic elimination procedure (AEP) which we use to derive a "reduced" one-body dynamics of the reference element u_1. The AEP is well rooted in the statistical physics repertoire [16,21,22]. As we shall see, the AEP yields a description that agrees well with the full dynamics in restricted regimes of parameter space. Outside these regimes, the AEP often provides a qualitative description of the system dynamics adequate to guide the selection of the coupling coefficients J_{ij} for optimum performance of the network.

An adiabatic condition on ω analogous to that in (2) is also essential in deriving the theoretical expressions [17,18] for the power spectral density of the reference element motion, from which we obtain SNR's,

$$U_1''(u_{1s\pm}) \ll \omega. \quad (4)$$

This condition enables one to write down a simple expression for a Kramers rate based on an adiabatically modulated potential barrier height. For the Kramers rate expression to be valid, the modulation of the potential barrier height must be much less than the noise spectral density, which in turn must be much less than the unmodulated potential barrier height U_0,

$$qc \ll D \ll U_0, \quad (5)$$

where c is half the separation of the minima of the unmodulated potential. The condition on the weak forcing

amplitude q also ensures that the modulation of the potential is not strong enough to force the reference element to switch between its two potential wells without the help of the noise. This condition of no deterministic switching is an important ingredient of stochastic resonance. The condition also allows the use of perturbation theory in the power spectral density calculation.

The theoretical power spectral density calculation is based on motion between the potential wells; it ignores motion within the wells. Therefore, it is not valid for very low noise strengths D, where intrawell motion dominates the dynamics.

The procedure for simplifying the system (1) has been described elsewhere [14,23] for somewhat different system configurations. In particular, in [23] we considered fluctuating coupling coefficients, monostable bath elements, and no deterministic signal. In [14] we considered independent additive noise at each element.

We now outline the procedure as it pertains to the system at hand. The starting point is the N-body Fokker-Planck equation (FPE) for the probability density function $P(u_1, u_2, \ldots, u_N; t)$,

$$\frac{\partial P}{\partial t} = \sum_i \left[-\frac{\partial}{\partial u_i}(Q_i P) + \frac{D}{2} \sum_j \frac{\partial^2 P}{\partial u_i \partial u_j} \right], \tag{6}$$

where the drift coefficient is

$$Q_i(u_1, u_2, \ldots, u_N) \equiv -\frac{u_i}{R_i} + J_{ii} \tanh u_i + \sum_{k \neq i} J_{ik} \tanh u_k + q \sin \omega t. \tag{7}$$

We factor the probability density function,

$$P(u_1, u_2, \ldots, u_N) = h(u_2, u_3, \ldots, u_N \mid u_1) g(u_1) \tag{8}$$

(suppressing t to simplify our notation), where h is to be interpreted as a conditional probability density for finding $u_{j>1}$ given u_1 (both h and g are normalized to have unit weight). The constraints (2) and (3) imply that we may substitute the factored probability density function (8) into the original FPE (6) and separate the slow variable u_1 from the fast one(s) [14,16,23],

$$\frac{\partial h}{\partial t} = \sum_{i>1} \left[-\frac{\partial}{\partial u_i}(Q_i h) + \sum_{j>1} \frac{D}{2} \frac{\partial^2 h}{\partial u_i \partial u_j} \right], \tag{9}$$

$$\frac{\partial g}{\partial t} = -\frac{\partial}{\partial u_1} [A(u_1) g(u_1)] + \frac{D}{2} \frac{\partial^2 g}{\partial u_1^2}, \tag{10}$$

with the kernel $A(u_1)$ defined by

$$A(u_1) \equiv \int \cdots \int h(u_2, u_3, \ldots, u_N \mid u_1) \times Q_1(u_1, u_2, \ldots, u_N) du_2 du_3 \cdots du_N. \tag{11}$$

In deriving (9) and (10) we have assumed that derivatives of h with respect to u_1 may be neglected compared to derivatives with respect to $u_{i>1}$. This follows from the slaving assumptions (2) and (3) [16].

We first must solve (9) in the long-time limit. Equation (2) allows us to treat u_1 as varying only adiabatically. For the purposes of integrating (9), therefore, we assume the modulation term to be constant. Far more serious is the lack of detailed balance [21] when the dimensionality of (9) exceeds unity. In general, a steady state (potential function) solution of (9) cannot be found for this case, although a local-equilibrium assumption for the bath permits us to write down an equilibrium bath density function as a superposition of Gaussians [23]. In what follows, we explicitly derive the solution for the $N = 2$ case, treating separately the cases of a monostable and bistable-bath element. We then discuss the extension of this solution to $N > 2$. We shall set $C_i = 1$ for convenience.

The long-time solution of (9) may be expressed as the negative exponential of a potential function,

$$\frac{D}{2} U(u_2) = \frac{u_2^2}{R_2} - 2J_{22} \ln(\cosh u_2) - 2u_2 J_{21} \tanh u_1 - 2u_2 q \sin \omega t, \tag{12}$$

which has two minima for $J_{22} > R_2^{-1}$ and J_{21} and q sufficiently small (3); otherwise it has only one minimum. The extrema may be determined by expanding about their counterparts for the uncoupled case [assuming coupling small compared to the self-coupling coefficient J_{22}, (3)]. We find that at

$$u_{2u} \approx \frac{R_2 J_{21} \tanh u_1 + R_2 q \sin \omega t}{1 - J_{22} R_2}, \tag{13}$$

the potential (12) has a maximum if double welled and a minimum otherwise. If double welled, the potential also has minima at

$$u_{2s\pm} \approx \pm u_{20} + \frac{R_2 J_{21} \tanh u_1 - R_2 q \sin \omega t}{1 - J_{22} R_2 \operatorname{sech}^2 u_{20}}, \tag{14}$$

with $\pm u_{20} \approx \pm J_{22} R_2 \tanh(J_{22} R_2)$ being the minima in the bath element potential in the absence of coupling and forcing.

Now consider the monostable-bath case ($J_{22} \leq R_2^{-1}$), for which the potential has a minimum at u_{2u}. We may replace the expression (12) by a second-order expansion about u_{2u},

$$U(u_2) \approx U(u_{2u}) - \frac{(u_2 - u_{2u})^2}{2} \frac{\partial^2 U}{\partial u_2^2}(u_{2u}), \tag{15}$$

thereby obtaining for the normalized bath probability density function

$$h(u_2 \mid u_1) = \sqrt{a/\pi} e^{-a(u_2 - u_{2u})^2}, \tag{16}$$

where $a \equiv D^{-1}(R_2^{-1} - J_{22} \operatorname{sech}^2 u_{20})$. It is apparent that we have replaced the actual bath probability density function by a Gaussian centered at the stable fixed point, since the bath element may be assumed to be at or near its adiabatically steady state because of the slaving assumption. After expanding $\tanh u_2$ about u_{2u} we

can evaluate the integral in (11) (the linear term in the $\tanh u_2$ expansion does not contribute to this integral). This leads to "effective" or reduced dynamics corresponding to the slow variable u_1 in the decoupled form

$$\dot{u}_1 = A(u_1) + \sqrt{D}\xi(t), \tag{17}$$

where

$$A(u_1) = -\frac{u_1}{R_1} + \left[J_{11} + J_{12}\left(1 - \frac{\mathrm{sech}^2 u_{2u}}{2a}\right)\right]\tanh u_1 + q\sin\omega t. \tag{18}$$

It is possible to simplify further this expression by separating out the trignometric function; this is achieved by an expansion of $\mathrm{sech}^2 u_{2u}$ for small q. After some calculation, we finally arrive at a more attractive expression for $A(u_1)$,

$$A(u_1) \approx -\frac{u_1}{R_1} + (J_{11} + J_{12}J_{21}b_2)\tanh u_1 + (1 + J_{12}b_2)q\sin\omega t, \tag{19}$$

where

$$b_2 \equiv \frac{R_2}{1 - J_{22}R_2}\left(1 - \frac{DR_2/2}{1 - J_{22}R_2}\right). \tag{20}$$

Subject to the constraints employed in the derivation, the reduced dynamics (17) should reproduce the dynamics of the coupled system on a coarse-grained scale, for the case of a monostable bath element u_2. By this we mean that individual trajectories $u_1(t)$ derived from (17) and the full dynamics (1) will not necessarily follow one another, but averaged quantities such as long-time probability density functions and power spectra should be the same for the two descriptions, in the appropriate regimes of parameter space.

For the case of a bistable bath element ($J_{22} > R_2^{-1}$), the derivation of the reduced dynamics follows an analogous route, except that we now expand the potential function about the two minima (14). We are effectively assuming that at long times the bath probability density function consists of two Gaussians centered at the minima. After some calculation, we readily obtain for this case,

$$h(u_2 \mid u_1) = \frac{e^{U(u_{2s+})}e^{-a_+(u_2 - u_{2s+})^2} + e^{U(u_{2s-})}e^{-a_-(u_2 - u_{2s-})^2}}{\sqrt{\pi/a_+}e^{U(u_{2s+})} + \sqrt{\pi/a_-}e^{U(u_{2s-})}}, \tag{21}$$

where we have defined $a_\pm = D^{-1}(R_2^{-1} - J_{22}\mathrm{sech}^2 u_{2s\pm})$. As in the monostable case we carry out an expansion of $\tanh u_2$ about the minima and carry out the integration in (11). It is instructive to write down explicitly the result of this integration, because it requires further simplification before it can be cast into a form that is suitable for our purposes. We obtain

$$I \equiv \int_{-\infty}^{\infty}\tanh u_2 h(u_2 \mid u_1)du_2 = \frac{1}{\mathcal{N}}\sqrt{\frac{\pi}{a_+}}e^{U(u_{2s+})}\tanh u_{2s+}\left(1 - \frac{\mathrm{sech}^2 u_{2s+}}{2a_+}\right) + \frac{1}{\mathcal{N}}\sqrt{\frac{\pi}{a_-}}e^{U(u_{2s-})}\tanh u_{2s-}\left(1 - \frac{\mathrm{sech}^2 u_{2s-}}{2a_-}\right), \tag{22}$$

where $\mathcal{N}$ is the normalization of the density function [denominator of (21)]. Equations (2) and (3) generally ensure $\mathrm{sech}^2 u_{2s\pm} \ll 2a_\pm$, guaranteeing convergence of the integral I.

In the interest of analytical tractability we now assume that the minima $u_{2s\pm}$ are very close to their locations $\pm u_{20}$ for the uncoupled and unforced case; i.e., we assume weak coupling and a small modulation amplitude q, as was done in the derivation of (19) for the monostable-bath case. To a first approximation, therefore, we replace $u_{2s\pm}$ by $\pm u_{20}$ in the expression for the integral I. After some calculation we find,

$$A(u_1) \approx -\frac{u_1}{R_1} + J_{11}\tanh u_1 + q\sin\omega t + J_{12}(\tanh u_{20}) \times \left(1 - \frac{DR_2/2}{1 - J_{22}R_2\mathrm{sech}^2 u_{20}}\mathrm{sech}^2 u_{20}\right) \times \tanh\left[2D^{-1}(J_{21}u_{20}\tanh u_1 + qu_{20}\sin\omega t)\right]. \tag{23}$$

A further simplification (strictly valid only in the large noise case) yields an expression having the structure of (19),

$$A(u_1) \approx -\frac{u_1}{R_1} + (J_{11} + J_{12}J_{21}b_2^{\mathrm{bi}})\tanh u_1 + (1 + J_{12}b_2^{\mathrm{bi}})q\sin\omega t, \tag{24}$$

where

$$b_2^{\mathrm{bi}} = 2D^{-1}(u_{20}\tanh u_{20}) \times \left(1 - \frac{DR_2/2}{1 - J_{22}R_2\mathrm{sech}^2 u_{20}}\mathrm{sech}^2 u_{20}\right). \tag{25}$$

For the bistable case, therefore, the reduced or effective dynamics are given by (17) with (23) or (24).

For future consideration, it is convenient to write the reduced dynamics (17) in the form

$$\dot{u}_1 = -\frac{dU(u_1)}{du_1} + \sqrt{D}\xi(t), \tag{26}$$

where we have introduced the potential function that affords us a more elegant mathematical treatment of the

dynamics,

$$U(u_1) \equiv \tfrac{1}{2}\alpha u_1^2 - \beta \ln\cosh u_1 - u_1 \delta \sin\omega t, \tag{27}$$

and we identify α, β, and δ with the appropriate expressions in the kernel $A(u_1)$ given by the reduced forms (19) or (24), depending on whether the bath element is monostable or bistable. Therefore, we have defined $\alpha \equiv (R_1 C_1)^{-1}$ and, if the bath elements are monostable,

$$\beta \equiv \frac{1}{C_1}\left(J_{11} + \sum_{i>1} J_{1i} J_{i1} b_i\right) \tag{28}$$

and

$$\delta \equiv \frac{q}{C_1}\left(1 + \sum_{i>1} J_{1i} b_i\right), \tag{29}$$

where

$$b_i \equiv \frac{R_i J_{1i} J_{i1}}{1 - J_{ii} R_i}\left(1 - \frac{D R_i}{2C_i(1 - J_{ii} R_i)}\right), \quad (i > 1). \tag{30}$$

We have included the C_i for generality.

Based on our previous work [23] we feel that (26)–(29) adequately describe the effective dynamics for the case of monostable bath elements for $N > 2$. However, for the bistable-bath case, such a generalization to the N-body case has not yet been derived.

The potential $U(u_1)$ will be bistable for $\beta > \alpha$, which is the case that is considered throughout this work. It is centered at $u_1 \approx 0$, with minima located at $c_\pm \approx \pm\frac{\beta}{\alpha}\tanh\frac{\beta}{\alpha}$. The modulation shifts these extrema slightly, and the shift can be computed by an expansion analogous to that carried out above for the bath element. The height of the potential barrier depends directly on the parameter β. It is worth noting that the effects of the bath and noise enter directly into the "effective" coefficients β and δ. This fact will be exploited in the following sections to optimize the system response. Note, finally, that terms arising from intrabath coupling are $\mathcal{O}(R_i C_i R_j C_j/(R_1 C_1)^2)$ $(i, j > 1)$ or higher and are negligible; they have been excluded from (28) and (29). It is also important to realize that although the bath density functions (16) and (21) yield reasonably good long-time behavior in the strictly monostable- or strictly bistable-bath regime, they do not provide a good description of the bath dynamics in the transition regime $\beta \approx \alpha$. In this regime, the bath is, in fact, undergoing a pitchfork bifurcation that characterizes the transition between mono- and bistability, and only a complete nonequilibrium characterization of the dynamics would be expected to yield good results.

Having obtained the reduced dynamics (26), we may apply the adiabatic theory of reference [17] and compute the power spectral density (PSD) of the variable u_1, whence the output SNR may be obtained. The spectrum consists of a broadband noise background and a δ-function spike at the signal frequency,

$$\mathcal{S}(\Omega) = N(\Omega) + S\delta(\Omega - \omega). \tag{31}$$

Harmonics, which would appear at odd multiples of the signal frequency, are not captured by this first-order approximation. The one-sided, time-averaged power spectral density (in terms of angular frequency) of the noise is

$$N(\Omega) = \frac{1}{2\pi}\left[1 - \frac{8(r_0\zeta)^2}{4r_0^2 + \omega^2}\right]\frac{8r_0c^2}{4r_0^2 + \Omega^2}. \tag{32}$$

The signal power is

$$S = \frac{8(r_0\zeta c)^2}{4r_0^2 + \omega^2}. \tag{33}$$

Here c is half the separation of the minima of the unperturbed potential, $\zeta \equiv \delta c/D$ is a perturbation theory expansion parameter, and r_0 is the unperturbed ($\delta = 0$) Kramers rate, $(2\pi)^{-1}\sqrt{|U''(0)|U''(c)}\exp(-2U_0/D)$. U_0 is the height of the potential barrier separating the two wells of the bistable potential (measured from the bottom of the wells) when the modulation term, $u_1\delta\sin\omega t$, vanishes.

The output SNR, $\mathcal{R}$, is the ratio of the signal and noise powers in a narrow frequency range of width $\Delta\omega$ centered about the signal frequency ω,

$$\mathcal{R} = \frac{S}{\Delta\omega N(\omega)}. \tag{34}$$

We use this definition of SNR, rather than taking the ratio of all of the signal power to all of the noise power, because it is more relevant to signal processing applications.

Note that effects due to the noise and deterministic modulation appear in both the signal (33) and noise (32) terms, unlike the case for a linear system. Furthermore, by increasing the signal amplitude the first factor in the noise term can be made smaller in magnitude so that one obtains a decrease in the background noise power. Increasing the noise strength increases the Kramers rate r_0 while decreasing the expansion parameter ζ. The interplay of these two effects leads to the resonancelike curve for the SNR vs D. Although the theory is only strictly valid for $D \ll U_0$, it correctly predicts the location of the maximum in the SNR vs D curve at $D \approx U_0$.

In the following sections we present the results of large-scale numerical simulations of the fully coupled equations (1) as well as the reduced system. Our primary goal is to compute an output SNR vs input noise curve while examining the effects of increasing the number of elements N. We find that, for the monostable-bath case, one may straightforwardly extend our expression (19) to the case of more than one bath element, obtaining (28) and (29). This is not surprising in light of our previous calculations [14] in which we derived the long-time solution of the $(N-1)$-body FPE corresponding to the bath density function. For the case of the bistable bath, the extension to more than one bath element is not straightforward. A detailed calculation (along the lines of [23]) for the bath density function in the $N > 2$ case is beyond the scope of this paper. We have, however, numerically compared a simple generalization of the bistable-bath results (21)–(24) for $N > 2$ with simulations of the full dynamics (1);

the results seem to indicate that a straightforward generalization (as in the monostable-bath case) to $N > 2$ yields results in agreement with numerical simulations only for low to moderate values of the forward coupling coefficients. This is illustrated later in this work.

III. NUMERICAL SIMULATIONS: THE OUTPUT SNR

To supplement our analytical calculations, we also computed the system's output SNR via numerical integration of (1) using the modified Heun method [24]. In our case, the modified Heun algorithm actually reduces to the Euler-Maruyama scheme,

$$u_i(t) = u_i(t-\Delta t) + \left[-\frac{u_i(t-\Delta t)}{R_i} + \sum_{j=1}^{N} J_{ij} \tanh u_j(t-\Delta t) + q \sin \omega (t-\Delta t) \right] \Delta t + \sqrt{D}\Delta W, \tag{35}$$

where ΔW is a "Wiener increment," i.e., the change in the value of a Wiener process over a time interval Δt: a normally distributed random number with mean zero and standard deviation $\sqrt{\Delta t}$. As stated in the preceding section, coupling between bath elements should not greatly affect the system. Therefore, we also leave out coupling between bath elements in our simulations. Note that this is never a factor for the $N = 1$ or $N = 2$ simulations.

The theory applies to a system driven by ideal white noise, which has a constant power spectral density at all frequencies. In numerical calculations or physical experiments, there is always a limit to the bandwidth of signals considered. For example, when the time series representing the system variables is sampled every Δt seconds, the highest frequency that can be represented is known as the Nyquist frequency and is equal to one half the sampling rate, giving $\omega_{\text{Nyquist}} = \pi/\Delta t$ (in terms of angular frequency).

In the case of the continuous-time equations, the one-sided power spectral density (in terms of angular frequency) of the noise has a height D/π for all frequencies, while in the numerical simulations we approximate this physically idealized and unrealizable signal by a noise signal with a flat spectrum of height D/π from 0 to $\omega_{\text{cut}} = \omega_{\text{Nyquist}}$ and a height of zero outside this range. Note that ideal white noise is an infinite power signal, and, therefore, physically unrealizable, while the power in the band-limited noise we use in the simulations (actually the variance) is equal to the area under its PSD curve: $\sigma^2 = \omega_{\text{cut}} D/\pi$.

There are several time scales involved in our system: the driving frequency, the relaxation rates in the slow and fast elements, and the Kramers rate in the slow and fast elements. The fact that we have slow and fast elements with widely separated time constants implies that we have to consider a wide frequency bandwidth. Furthermore, we wanted to approximate white noise conditions, and we determined that the system was sensitive to noise energy at very high frequencies. Therefore, we generated extremely finely sampled time series with a time step such that $\omega_{\text{Nyquist}} = 4096\omega$. To avoid aliasing we maintained this sample rate throughout our computations. We also convolved the time series with a Welch window before computing the power spectra. Figure 1 shows the effect of noise bandwidth on output SNR. To generate this figure, we low-pass filtered the noise while keeping our time step size constant.

The small step size and the fact that we needed well-averaged PSD's from which to compute our SNR's required that we use a supercomputer. We chose the Intel Paragon, and distributed the job of generating time series and computing 1024 power spectra over, typically, 32 – 128 processors working in parallel. For $N = 2$, a 32-point curve of SNR versus noise strength can be generated in a few hours. For comparison, on a workstation (e.g., HP-Apollo 425T) with a moderately fast processor this computation would require well over a week.

First, we consider the case $J_{ii} \leq (R_i C_i)^{-1}$ $(i > 1)$ where the bath elements, if uncoupled, would be monostable. Guided by (29) and noting that $b_i > 0$ $(i > 1)$ we choose $J_{1i} > 0$ $(i > 1)$ to increase the effective signal amplitude and thus the output SNR. Similarly, (28) implies we can choose $J_{i1} < 0$ $(i > 1)$ to decrease β, reducing the effective barrier between the two potential wells. We have given each $J_{i>1,1}$ a unique value so that each bath element evolves uniquely. However, setting all these coupling coefficients equal (or, equivalently, setting $N = 2$ and multiplying J_{21} appropriately) gives very nearly the same output SNR.

In Fig. 2, we show the output SNR [computed from the time series $u_1(t)$] for systems of one to ten elements, with the bath elements being monostable. For comparison we

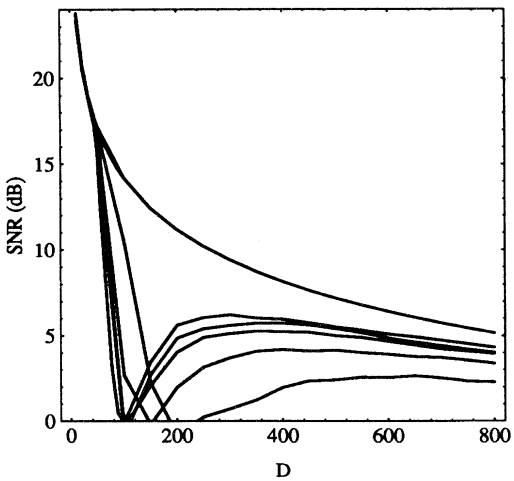

FIG. 1. Sensitivity to noise bandwidth. Uppermost curve: Input SNR. Lower curves (lowest to highest): output SNR for noise bandwidths of 32ω, 64ω, 128ω, 256ω, and 4096ω. $N = 1$. $R_1 = 0.018\,6916$. $C_1 = 1$. $J_{11} = 216$. $q = 8$. $\omega = 1.22522$. $\Delta\omega = \omega/32$.

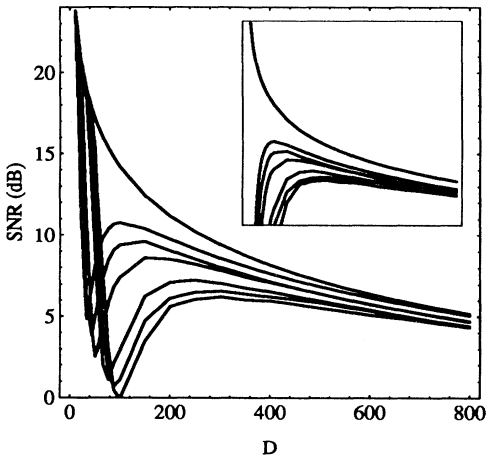

FIG. 2. Monostable bath. Uppermost curve: Input SNR. Lower curves (lowest to highest): Output SNR for $N = 1$, 2, 3, 6, 8, 10. Main plot: analog output. Inset: binary output. (Main plot and inset have the same coordinate ranges.) $R_{i>1} = 0.001$. $C_{i>1} = 1$. $J_{ii} = 100$ $(i > 1)$. $J_{1,i>1} = 50$. $J_{\{2,3,\ldots,10\},1} = \{-50, -55, -45, -52, -48, -54, -46, -53, -47\}$. $J_{ij} = 0$ $(i, j > 1; i \neq j)$. Other parameters as in Fig. 1.

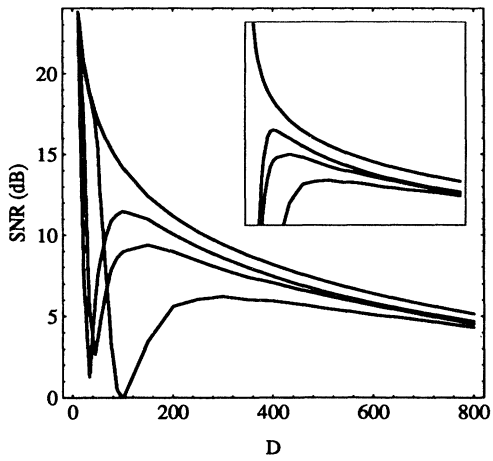

FIG. 3. Bistable bath. Uppermost curve: input SNR. Lower curves (lowest to highest): output SNR for $N = 1$, 2, 3. Main plot: analog output. Inset: binary output. (Main plot and inset have the same coordinate ranges.) $J_{ii} = 1500$ $(i > 1)$. Other parameters as in Fig. 2. Note: sharp minima of the $N = 2, 3$ curves not fully resolved by points plotted.

also plot the input SNR, $(q^2/2)/(\Delta\omega D/\pi)$, with $\Delta\omega$ being the frequency resolution of our power spectra. As we increase the number of elements, the output SNR at moderate noise levels also increases. This effect derives from our choice of couplings. The inset illustrates an even greater coupling effect: it shows the enhancement in the output SNR of a hypothetical transducer that has the same internal dynamics as our reference element but has a binary (rather than analog) output, $\mathrm{sgn}[u_1(t)]$.

For the case of $\sum_{i>1} J_{1i}$ not too large (e.g., for the $N = 1$, 2, and 3 curves of Fig. 2) the numerical simulations and the theory agree quantitatively. The output SNR for these cases is well quantified by the theory, and its maximum occurs at a critical noise value approximately equal to the solution of the transcendental equation $D = U(0) - U(c)$, as predicted by the theory [17]. For larger values of $\sum_{i>1} J_{1i}$ $(N = 8, 10)$, the theory, while still in qualitative agreement with simulations, predicts an output SNR that exceeds the input SNR for a range of noise strengths. In contrast, the simulations show that the output SNR approaches but does not exceed the input SNR. The discrepancy between theory and simulation can be traced to a breakdown of the conditions required for its derivation.

Figure 3 compares the output SNR from systems of one to three elements, with the bath elements chosen to be bistable in isolation $[J_{ii} > (R_i C_i)^{-1}$ $(i > 1)]$. As in the monostable case, at moderate noise levels the output SNR increases with N, causing the SNR gain to approach unity.

Figure 4 illustrates the implications of systematically abandoning the slaving principle in a two element system by increasing R_2. We see that increasing R_2 causes the SNR gain to approach unity at moderate noise levels. The *highest* output SNR in Fig. 4 occurs for $R_2 = R_1$. This is intriguing because it suggests that arrays of elements with comparable time constants perform very well. In fact, if we additionally set $J_{22} = J_{11}(= 216)$, so that we have a pair of identical elements (distinguished only by their opposite couplings to each other), we get an output SNR only 1 dB lower at the SR maximum. This offers promise for applications where arrays might be easier to construct if all the elements are the same.

In Figs. 2–4 the output SNR exhibits the characteristic dependence on the input noise that is taken to be the hallmark of SR: At very low noise levels the effective

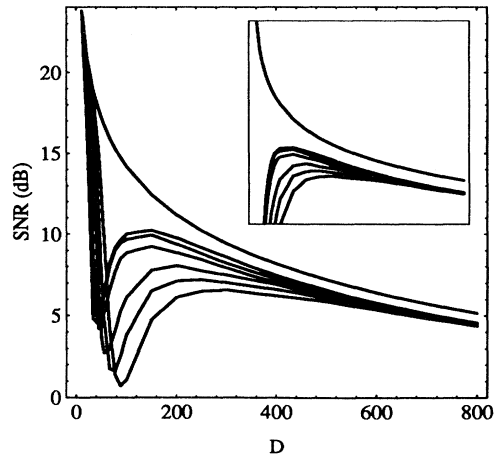

FIG. 4. Abandoning the slaving principle by increasing the time constant of the bath element until it equals that of the reference element. N=2. Uppermost curve: input SNR. Lower curves (lowest to highest): output SNR for $R_2 = 0.001$, 0.002 45, 0.004 245, 0.008, 0.012, 0.018 6916 $(= R_1)$. Main plot: analog output. Inset: binary output. (Main plot and inset have the same coordinate ranges.) Other parameters as in Fig. 2.

dynamics are bistable, but the state point is confined to the bottom of a single well of the potential for many periods of the driving signal [17]. The shape of the potential at the bottom of the wells is approximately parabolic, i.e., that of a harmonic oscillator. Consequently, the response of the analog-output system is nearly linear, with the output SNR approaching the input SNR as $D \to 0$. The binary output SNR goes to zero as $D \to 0$ because without help from noise, the sinusoidal input is too weak to cause interwell hopping. With increasing noise, the output SNR goes through a minimum (for the analog output) followed by a maximum where the noise enhances interwell transitions in phase with the driving signal (SR) [17]. Additional noise tends to minimize the potential barrier's significance, returning us to the scenario of motion in the bottom of a single, approximately parabolic, potential well (albeit a much larger one).

Observe from (28) and (30) that for $N > 1$ the barrier height of the effective potential (27) as well as the locations $\pm c$ of its wells are functions of the noise. Hence, at each point on the SNR curves, the noise systematically alters the effective potential. However, the dominant effects on the potential are the result of the coupling, which reduces the effective potential barrier height so that even at moderate noise levels the potential tends to a parabola. The effective dynamics may be said to be "linearized" by a combination of the noise (an effect that has also been observed in a single bistable element [25]) and the coupling. The effect is qualitatively similar to that observed at extremely low and high noise levels insofar as the dynamics tends to that of the simple harmonic oscillator and the output SNR approaches the input SNR. This is the central point of this paper: *for moderate input noise levels, the SNR at the output of a nonlinear dynamic element can be brought closer to the response of a linear system by incorporating the element into a coupled array.*

Limitations of the theoretical description

Our theoretical calculations involve several levels of approximation. First, we use adiabatic elimination to reduce a system of N coupled differential equations to an equation in one variable [Eqs. (17) with (18) or (23)]. This approximation predicts that the long-time solution of the Fokker-Planck equation of the reference element, a phase-dependent probability density function, is the same as that of the FPE of a one-variable equation. We can test the accuracy of this approximation by comparing the phase-dependent probability density functions of the time series of the simulated N-variable and reduced one-variable systems. Figure 5 shows this comparison for a bistable-bath system. As we increase $J_{1,i>1}$, the difference between the solutions of the three-variable and one-variable FPE's grows. This is not surprising, since the $J_{1,i>1}$ multiply terms in the $N = 3$ generalization of (23) which are only approximations.

The second approximation allows us to cast the reduced one-variable system in the form of system (1) with $N = 1$. This approximation works well for monostable-bath systems. We illustrate the accuracy of this approximation by comparing the phase-dependent probability density functions of the time series of the simulated N-variable and the two one-variable systems. Figure 6 shows the effects of the first and second approximations for a monostable-bath system. The first approximation gives good agreement, and adding in the second approximation does not significantly worsen the agreement.

A third approximation in our theory occurs when we use the approach of [17] to compute the output SNR based on the shape of the potential. We illustrate this in Figure 7, where we compare the SNR resulting directly from a simulation of the N-variable system (1), the SNR's resulting from simulations of the reduced one-variable system (17) and (18) as well as the simplified system using (19). We also plot on this figure the theoretical SNR obtained by applying the approach of [17] to the simplified system to obtain (32)–(34). The four curves are seen to be in very good agreement.

IV. TUNING SYSTEM PARAMETERS

A positive (negative) coupling corresponds to an excitatory (inhibitory) synapse in a neural network, or a ferromagnetic (antiferromagnetic) interaction in a magnetic spin system. The signs of the coupling terms affect whether coupling will increase or decrease the output SNR of the reference element. As mentioned earlier, choosing $J_{1,i>1} > 0$ and $J_{i>1,1} < 0$ gives the greatest SNR enhancement. Figure 8 illustrates this effect. In fact, the theory correctly predicts the relative positions

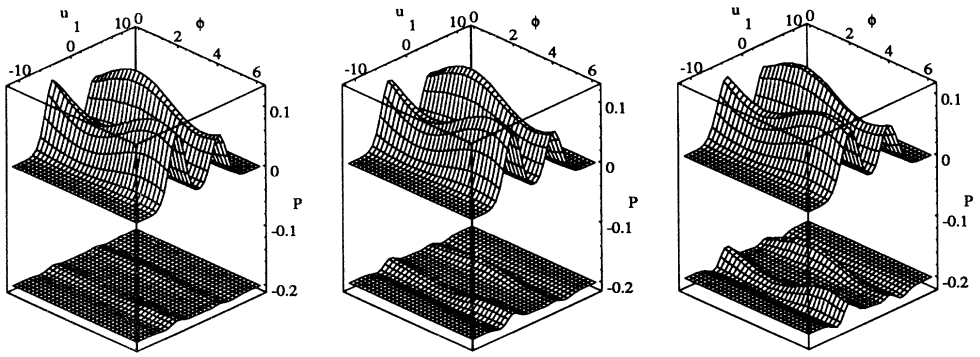

FIG. 5. The upper surface of each pair shows the phase-dependent probability density $P(u_1, \phi)$ for the bistable-bath $N = 3$ system. The lower surface shows the difference between the $N = 3$ system (1) and the reduced one-variable system (17) and (23), using the same scale, but offset by -0.2. From left to right, $J_{1,i>1} = 5$, 10, 20. $J_{ii} = 1500$ $(i > 1)$. $D = 200$. $\phi \equiv \omega t \mathrm{mod} 2\pi$. Other parameters as in Fig. 2.

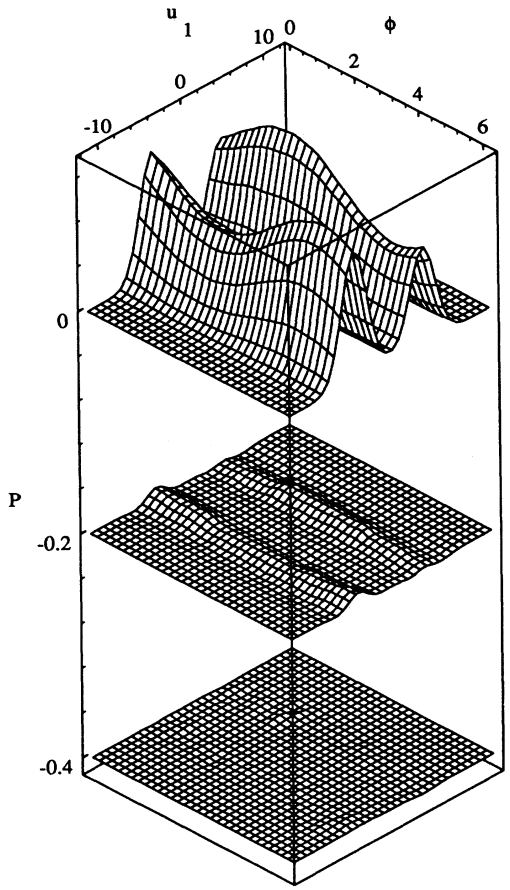

FIG. 6. Upper surface: phase-dependent probability density $P(u_1, \phi)$ for the monostable-bath $N = 2$ system. Middle surface: difference between the $N = 2$ system (1) and the reduced one-variable system (17), (18), offset by -0.2. Lower surface: difference between the reduced one-variable system and the simplified $N = 1$ system (19), (26)–(29), offset by -0.4. $D = 200$. $\phi \equiv \omega t \mathrm{mod} 2\pi$. Other parameters as in Fig. 2.

of all the curves in the figure.

The output SNR shows a maximum not only as noise strength is varied, but also as we vary several of the system parameters. Figure 9 shows tuning of the system by varying the interelement coupling strengths. The fact that there is an optimal coupling strength for maximizing the output SNR agrees with what we have seen in chains of Duffing oscillators with local linear coupling, making it a robust phenomenon [26,27]

Figure 10 shows tuning as a function of bath element self-coupling, J_{22}. The SNR passes through a maximum as a function of J_{22}. Another interesting phenomenon is apparent when we compare the results for the two values of J_{12} shown. For $J_{12} = 100$, the (binary output) SNR surface has an absolute maximum, while for $J_{12} = 251$ it approaches infinity as $D \to 0$ with $J_{22} \approx 1000$. The difference is that for the higher J_{12} value, the motion in the bath oscillator can "deterministically" switch the reference oscillator. For $J_{22} \leq 1000$, the isolated bath oscillator potential has a single well. The bottom of the

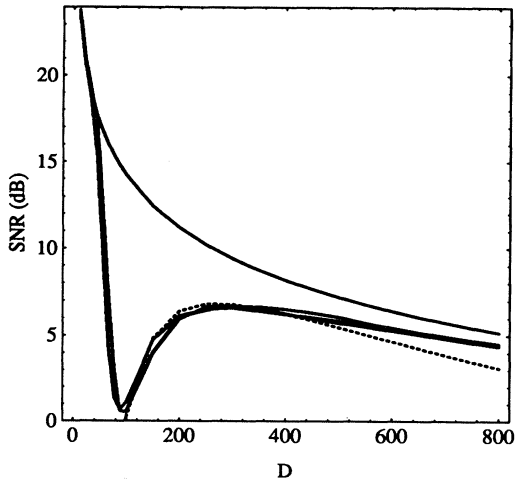

FIG. 7. Testing theoretical prediction of SNR. Uppermost curve: input SNR. Solid lower curves: output SNR of $N = 2$ system [by simulation of (1)], reduced one-variable equations (17) and (18), and simplified one-variable equations (17) and (19). Dotted curve: theoretical computation of output SNR of $N = 2$ system using (32)–(34). Parameters as in Fig. 2.

well is quite flat for $J_{22} \approx 1000$. This motion gets amplified by the large coupling strength and deterministically switches the reference element. Indeed, in the absence of coupling the reference oscillator switches deterministically for $q > 117$. Of course, when deterministic switching occurs we no longer see a stochastic resonance.

V. DISCUSSION: THEORETICAL LIMIT ON IMPROVING SNR

The output SNR alone is not a complete measure of the performance of a signal processing system. For signal estimation, relevant performance measures are mean

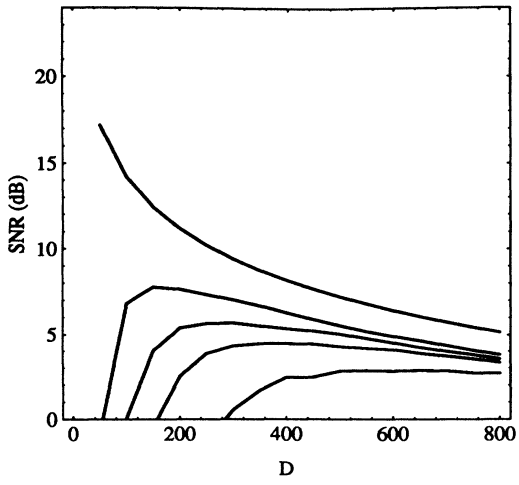

FIG. 8. Effect of signs of couplings. Uppermost curve: input SNR. Lower curves (lowest to highest): Output SNR for $(J_{12}, J_{21}) = \{(-200, -100), (-200, +100), (+200, +100), (+200, -100)\}$. $N = 2$. Other parameters as in Fig. 2.

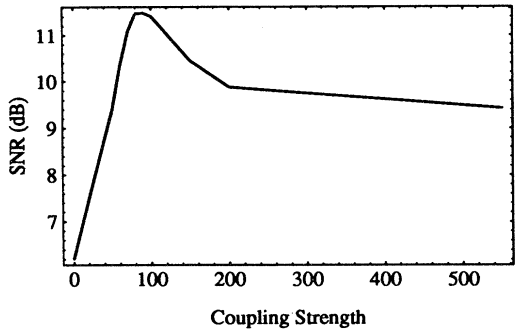

FIG. 9. Coupling tuning curve. Maximum SNR as a function of coupling strength J_{12}. $N = 2$. $J_{22} = 1500$. Other parameters as in Fig. 2.

square error or Bayesian tests [3]. For example, a nonlinear signal processor may output a signal that has infinite SNR but is useless because it has no correlation with the input signal. Such a system would be one which simply generates a sine wave at the signal frequency, totally ignoring its input. For signal detection, one must consider detection statistics: probability of detection and probability of false alarm. Such statistics may be summarized in plots of detection probability versus false alarm probability, known as receiver operating characteristic (ROC) curves. Presenting ROC curves is beyond the scope of this paper; however, we have found that the ROC curves follow the SNR curves, exhibiting a maximum in performance at a critical noise strength [27].

The optimal filter for detecting a known signal in Gaussian white noise is the correlation receiver or matched filter, which is a linear filter whose output is compared to a threshold [3]. The optimal estimator of a linearly modulated signal in Gaussian white noise is also a linear filter [3]. For linear filters, the output SNR equals the input SNR if the SNR's are measured in a sufficiently narrow band around the signal frequency. This suggests why a stochastic resonator circuit driven by a sine wave in Gaussian white noise has an output SNR bounded by the SNR obtained by a linear filter; i.e., the input SNR.

On the other hand, the output SNR of a nonlinear filter *may* exceed its input SNR. The bandpass limiter is a circuit that illustrates this effect. It consists of a bandpass filter followed by a threshold (or infinite limiter) circuit. The bandpass filter removes all signals outside a narrow band around the signal frequency, and the threshold circuit converts the analog output of the bandpass filter to a two-level output ($+V$ if the bandpass filter output is positive, $-V$ if negative). This nonlinear device improves the SNR of a signal by tacitly assuming that the signal power exceeds the noise power. When the assumption holds, the SNR increases by several dB. However, when the assumption fails, the SNR decreases slightly [28]. The fact that there is a positive SNR gain only above a cer-

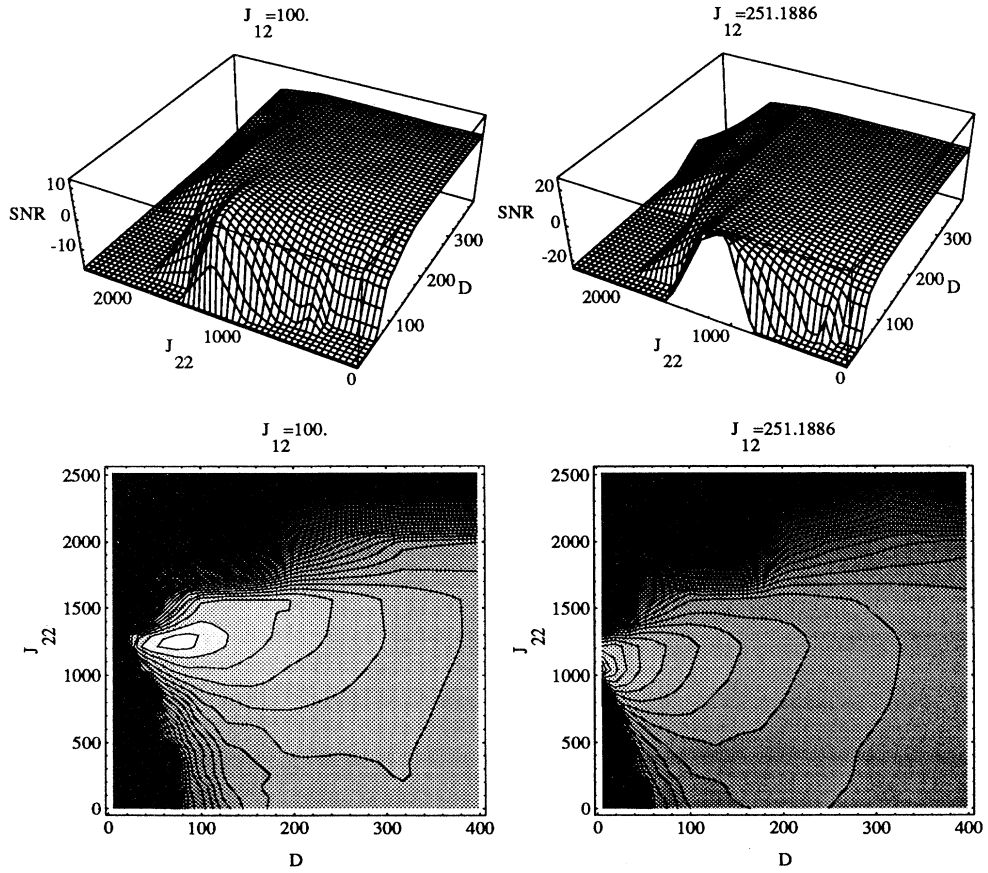

FIG. 10. Binary-filtered output SNR as a function of noise strength D and self-coupling J_{22}, displayed as surface and contour plots for two values of J_{12}. $N = 2$. Other parameters as in Fig. 2.

tain threshold input SNR (the "threshold effect") is a universal phenomenon generic to all nonlinear processors [3].

When we drive one of our bistable nonlinear dynamic elements with a sine wave plus noise that has most of its energy concentrated around the signal frequency, the system should behave somewhat like the bandpass limiter. The limiting effect is due to the hyperbolic tangent function. In Figure 11, we see evidence of two threshold effects: one concerning q and one concerning both q and D. First, if the signal strength q is too low, positive SNR gain is not possible. Second, even for larger values of q, we see that significant SNR gain does not occur if the input SNR is too low. This second effect corresponds to the threshold effect seen in the bandpass limiter.

Gang *et al.*, have also observed a positive SNR gain for a stochastic resonance circuit driven by band-limited noise [9]. Similar gains have been predicted by Hänggi *et al.* for the driven Kramers equation at moderate to large friction [8], and by Kiss [13] in a threshold element subject to an aperiodic signal in noise.

Another factor affecting SNR enhancement in coupled arrays is whether the noise at different elements is correlated or uncorrelated. In this work, we have considered the case of correlated (in fact, identical) noise at each element. This corresponds to the situation where noise is coming from an external source. This is the most challenging situation in which to try to enhance output SNR by using a coupled array. To see why, consider the situation where the noise at different elements is uncorrelated [26,27,29,30]. This happens, for example, when the noise comes from sources internal to each element. In this case, using many elements, coupled or not, and summing their outputs enhances SNR because signal components add coherently, while (uncorrelated) noise components add incoherently. In the correlated-noise case, one does not have this effect to exploit, so it is rather surprising that coupling enhances SNR in this case at all. But we have seen that it does, and in fact this effect also contributes to enhancing the output SNR in coupled arrays with uncorrelated noise [26,27].

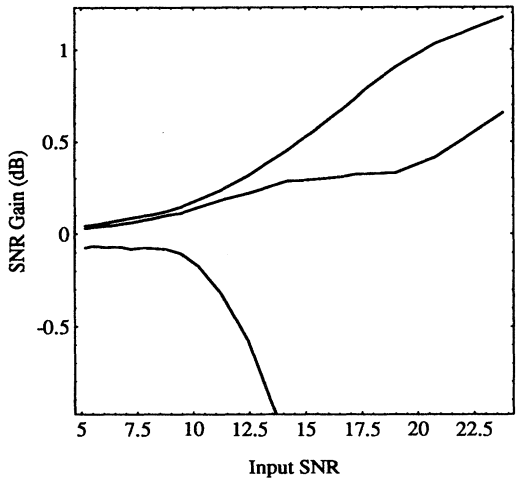

FIG. 11. Output SNR may exceed input SNR for bandpass-filtered noise (pass band: 0.72ω to 1.3ω). For each curve, signal strength q was held fixed, while noise strength D was varied. From lowest to highest, $q = 120$, 240, 480. Other parameters as in Fig. 1.

Linear versus nonlinear coupling can also make a great deal of difference in certain cases. With uncorrelated noise, linear coupling of the form $J_{ij}(u_i - u_j)$ can boost the SNR of the response of an element coupled into a chain, and in fact synchronizes the elements of the chain when the noise strength is at the value that maximizes the SNR [26,27]. However, such linear coupling has little to no effect on identical oscillators subject to *correlated* noise. In contrast, nonlinear coupling can completely remove oscillator nonlinearities for some configurations of identical oscillators subject to correlated noise. For example, this occurs for a system of the form (1) consisting of a pair of identical oscillators ($N = 2$, $C_1 = C_2$, $R_1 = R_2$, $J_{11} = J_{22}$) with couplings $J_{12} = J_{21} = -J_{11}$ and identical initial conditions on u_1 and u_2. In this case, the nonlinear coupling causes the two nonlinear elements to perform exactly like a linear system, which is optimal for signal-processing tasks.

Although the cases of correlated vs uncorrelated noise and linear vs nonlinear coupling differ, they still have much in common. The early work of Jung *et al.* [29] dealt with ensembles of linearly coupled bistable elements subject to uncorrelated noise. They observed a performance enhancement as a function of noise and/or coupling analogous to our results for nonlinear coupling and correlated noise.

VI. SUMMARY

We have seen that the performance (measured via output SNR) of a nonlinear dynamic system or device can be improved by coupling the device in an array, with the coupling coefficients carefully selected. Coupling makes the system as a whole respond more like a linear system over a range of noise strengths. Violating the slaving condition by increasing the time constants of the bath elements also appears to "linearize" the system, with the SNR gain approaching unity.

The optimal choice (with regard to magnitude and sign) of the coupling coefficients J_{1i}, J_{i1} ($i > 1$) appears to be that which brings about a cooperative increase in the effective amplitude δ and a decrease in the barrier height of the effective potential through a decrease in β. Even though the theory does not always provide an accurate prediction of the response of (1), it nonetheless provides a reliable guide to selecting the optimal coupling coefficients for enhanced response. Finally, we note that *both* the noise and the coupling contribute to the cooperative effect of enhanced response.

Can we apply coupling to practical systems? Nonlinear detectors of weak signals embedded in background noise exhibit SR: For example, Hibbs *et al.* [31] have shown that an rf superconducting quantum interference device

magnetometer operated in the hysteretic mode displays SR. SR-like effects have also been observed in sensory neurons [32] and predicted in simple models of neural dynamics [33,15]; this has followed speculation that noise may play a constructive role in the response of neural networks [34]. Coupling such nonlinear dynamic elements may enhance their output SNR. From a signal processing perspective, we have pointed out that a linear filter is optimal for detecting a sine wave in Gaussian white noise. Thus, the linearizing effect of replacing a single nonlinear dynamic element by a coupled array may help systems that rely on nonlinear detectors or transducers to approach optimal performance.

ACKNOWLEDGMENTS

We warmly acknowledge discussions with T. Albert and G. Schmera (San Diego), P. Hänggi (Augsburg), P. Jung (Illinois), L. Gammaitoni and F. Marchesoni (Perugia), D. Petracchi (Pisa), F. Moss (St. Louis), K. Wiesenfeld (Atlanta), and L. Kiss (Uppsala). Support from the Physics Division of the Office of Naval Research and NRaD's Internal Research Program is also gratefully acknowledged. M.E.I. acknowledges support from the National Research Council. This work was supported in part by a grant of HPC time from the DOD HPC Distributed Center at Wright-Patterson Air Force Base.

[1] P. Jung, Phys. Rep. **234**, 175 (1993); K. Wiesenfeld and F. Moss, Nature **373**, 33 (1995).

[2] Proceedings of the NATO Advanced Research Workshop on Stochastic Resonance in Physics and Biology, edited by F. Moss, A. Bulsara, and M. Schlesinger [J. Stat. Phys. **70** (1993)]; Proceedings of the International Workshop on Fluctuations in Physics and Biology: Stochastic Resonance, Signal Processing, and Related Phenomena, Elba, Italy, 1994, edited by R. Mannella and P. McClintock (unpublished).

[3] See, e.g., H. van Trees, *Detection, Estimation and Modulation Theory* (J. Wiley, New York, 1978).

[4] L. Gammaitoni, E. Menichaella-Saetta, S. Santucci, and F. Marchesoni, Phys. Lett. A **142**, 59 (1989).

[5] G. De-chun and H. Gang, Phys. Rev. A **46**, 3243 (1992).

[6] L. Gammaitoni (private communication).

[7] G. De-chun, H. Gang, W. Xia-dong, Y. Chun-yan, Q. Guang-ron, and L. Rong, Phys. Rev. E **48**, 4862 (1993); T. Albert, A. Bulsara, G. Schmera, and M. Inchiosa, in *Proceedings of the Twenty-seventh Asilomar Conference on Signals, Systems and Computers* (IEEE Society Press, Los Alamitos, CA, 1994).

[8] P. Hänggi, P. Jung, C. Zerbe, and F. Moss, J. Stat. Phys. **70**, 25 (1993).

[9] R. Li, G. Hu, C. Yang, X. Weng, G. Qing, and H. Zhu (unpublished).

[10] J. Grohs, S. Apanasevich, P. Jung, H. Ißler, D. Burak, and C. Klingshirn, Phys. Rev. A **49**, 2199 (1994).

[11] S. Rice, Bell Syst. Tech. J. **23**, 282 (1944); **24**, 46 (1945); **27**, 109 (1948); J. Bendat, *Principles and Applications of Random Noise Theory* (J. Wiley, New York, 1958); I. Blake and W. Lindsey, IEEE Trans. Inf. Theory **IT-19**, 295 (1973), and references therein.

[12] K. Wiesenfeld, D. Pierson, E. Pantazelou, C. Dames, and F. Moss, Phys. Rev. Lett. **72**, 2125 (1994); A. Bulsara, S. Lowen, and C. Rees, Phys. Rev. E **49**, 4989 (1994); Z. Gingl, L. Kiss, and F. Moss, Europhys. Lett. **29**, 191 (1995); P. Jung, Phys. Rev. E **50**, 2513 (1994); P. Jung and G. Mayer-Kress, Phys. Rev. Lett. **74**, 130 (1995); F. Moss, D. Pierson, and D. O'Gorman, Int. J. Bifurc. Chaos **4**, 1383 (1994).

[13] L. Kiss, in *Proceedings of the Third Technical Conference on Nonlinear Dynamics (Chaos) and Full Spectrum Processing*, edited by R. A. Katz (AIP, New York, in press).

[14] A. Bulsara and G. Schmera, Phys. Rev. E **47**, 3734 (1993); A. Bulsara and A. Maren, Biol. Cyb. **70**, 145 (1993); in *Rethinking Neural Networks: Quantum Fields and Biological Data*, edited by K. H. Pribram (Erlbaum, Hillsdale, NJ, 1993).

[15] A. Longtin, A. Bulsara, and F. Moss, Phys. Rev. Lett. **67**, 656 (1991); Nature **352**, 469 (1991); A. Bulsara and F. Moss, in *Proceedings of the Meeting on Noise in Physical Systems and 1/f Fluctuations ICNF91*, edited by T. Musha, S. Sato, and Y. Yamamoto (Omsha, Tokyo, 1991); A. Longtin, A. Bulsara, and F. Moss, Mod. Phys. Lett. B **6**, 1299 (1992); A. Longtin, Los Alamos National Laboratory, Report No. LA-UR-92-163, 1992 (unpublished); J. Stat. Phys. **70**, 309 (1993); A. Longtin, A. Bulsara, D. Pierson, and F. Moss, Biol. Cyb. **70**, 569 (1994).

[16] H. Haken, *Synergetics* (Springer Verlag, Berlin, 1977).

[17] B. McNamara and K. Wiesenfeld, Phys. Rev. A **39**, 4854 (1989).

[18] L. Gammaitoni, F. Marchesoni, E. Menichaella-Saetta, and S. Santucci, Phys. Rev. Lett. **62**, 349 (1989); Phys. Rev. A **40**, 2114 (1989).

[19] M. Inchiosa and A. Bulsara, Phys. Lett. A, **200**, 283 (1995).

[20] See, e.g., D. Amit, *Modeling Brain Function* (Cambridge University Press, London, 1989); G. Weisbuch, *Complex Systems Dynamics* (Addison Wesley, New York, 1991); J. Hertz, A. Krogh, and R. Palmer, *Introduction to the Theory of Neural Computation* (Addison Wesley, New York, 1991)

[21] C. Gardiner, *Handbook of Stochastic Methods* (Springer Verlag, Berlin, 1983); P. Grigolini and F. Marchesoni, in *Memory Function Approaches to Stochastic Problems in Condensed Matter*, edited by M. Evans (J. Wiley, New York, 1985).

[22] K. Kaneko, Prog. Theor. Phys. **66**, 129 (1981); H. Haken and A. Wunderlin, Z. Phys. **47**, 179 (1982); L. Luigiato, P. Mandel, and L. Narducci, Phys. Rev. A **29**, 1438 (1984); C. Festa, L. Fronzoni, P. Grigolini, and F. Marchesoni, Phys. Lett. A **102**, 95 (1984); G. Schoner and H. Haken, Z. Phys. **63**, 493 (1986); H. Fu, H. Haken, and A. Wunderlin, Z. Phys. **76**, 127 (1989); Z. Zhaojue, W. Schieve, and P. Das, Physica D **67**, 224 (1993).

[23] W. Schieve, A. Bulsara, and G. Davis, Phys. Rev. A **43**, 2613 (1991).

[24] T. C. Gard, *Introduction to Stochastic Differential Equations* (Marcel Dekker, Inc., New York, 1988).

[25] M. I. Dykman, D. G. Luchinsky, and R. Mannella, in *Fluctuations and Order: The New Synthesis*, edited by M. Millonas (Springer Verlag, New York, 1994).

[26] J. Lindner, B. Meadows, W. Ditto, M. Inchiosa, and A. Bulsara, Phys. Rev. Lett. (to be published).

[27] M. Inchiosa, A. Bulsara, J. Lindner, B. Meadows, and W. Ditto, in *Proceedings of the Third Technical Confer-*

ence on Nonlinear Dynamics (Chaos) and Full Spectrum Processing (Ref. 13).

[28] W. B. Davenport, Jr., J. Appl. Phys. **24**, 720 (1953).

[29] P. Jung, U. Behn, E. Pantazelou, and F. Moss, Phys. Rev. A **46**, R1709 (1991).

[30] E. Pantazelou, F. Moss, and D. Chialvo, in *Noise in Physical Systems and 1/f Fluctuations*, edited by P. Handel and A. Chung (AIP Press, New York, 1993).

[31] A. Hibbs, E. Jacobs, J. Bekkedahl, A. Bulsara, and F. Moss, in *Noise in Physical Systems and 1/f Fluctuations* (Ref. 30); A. Hibbs, E. Jacobs, J. Bekkedahl, A. Bulsara, and F. Moss, J. Appl. Phys. (to be published).

[32] J. Douglass, L. Wilkens, E. Pantazelou, and F. Moss, Nature **365**, 337 (1993); H. A. Braun, H. Wissing, K. Schäfer, and M. C. Hirsch, Nature **367**, 270 (1994).

[33] A. Bulsara, E. Jacobs, T. Zhou, F. Moss, and L. Kiss, J. Theor. Biol. **152**, 531 (1991).

[34] J. Buhmann and K. Schulten, Biol. Cyb. **61**, 313 (1987); D. Gardner, Neural Networks **2**, 69 (1989); M. Inchiosa, in *Noise in Physical Systems and 1/f Fluctuations* (Ref. 30).